

Strong effects of time-dependent ionization in early SN 1987A

Victor P. Utrobin^{1,2} and Nikolai N. Chugai³

¹ Max-Planck-Institut für Astrophysik, Karl-Schwarzschild-Str. 1, D-85741 Garching, Germany

² Institute of Theoretical and Experimental Physics, B. Chermushkinskaya St. 25, 117259 Moscow, Russia

³ Institute of Astronomy of Russian Academy of Sciences, Pyatnitskaya St. 48, 109017 Moscow, Russia

Received 23 December 2004 / accepted 16 March 2005

Abstract. We study a time-dependent hydrogen ionization in the atmosphere of SN 1987A during the first month after the explosion. The model includes kinetics of hydrogen ionization and excitation, molecular hydrogen kinetics, and a time-dependent energy balance. The primary strong effect of the time-dependent ionization is the enhanced hydrogen ionization compared to the steady-state model. The time-dependent ionization provides a sufficient population of excited hydrogen levels to account for the observed $H\alpha$ without invoking the external ^{56}Ni . We find that the Ba II 6142 Å line in SN 1987A can be reproduced for the LMC barium abundance. This resolves the long-standing problem of the unacceptably high barium overabundance in SN 1987A. The key missing factor that should be blamed for the "barium problem" is the time-dependent ionization. The modelling of the $H\alpha$ profile on day 4.64 indicates the ratio of the kinetic energy to the ejected mass $\approx 0.83 \times 10^{50} \text{erg } M_{\odot}^{-1}$.

Key words. stars: supernovae: individual: SN 1987A – stars: supernovae: type IIP supernovae

1. Introduction

Spectra of type IIP supernovae (SN) combined with photometric data are the primary source of our knowledge about the mass, energy, chemical composition, mixing, asymmetry of ejecta that are of a vital importance for the verification of the explosion mechanism. Generally, to recover the information imprinted in the spectra one needs to use rather elaborated models. Unfortunately, the ultimate model with all the physics included is beyond reach, so some simplifications are unavoidable. One of the assumptions accepted in the atmosphere models is the steady-state approximation for the ionization kinetics.

Yet, that the time-dependent effect of the hydrogen ionization may play a role in the SN envelope has been recognized by Kirshner & Kwan (1975); they applied this effect to account for the high $H\alpha$ luminosity of the type II SN 1970G. The time-dependent ionization has been exploited for SN 1987A to account for the high excitation of hydrogen in the outer atmosphere ($v > 7000 \text{ km s}^{-1}$) during the first 40 days (Chugai 1991a). The crucial role of the time-dependent ionization at the late nebular epoch of SN 1987A has been emphasized by Clayton et al. (1992) and Fransson & Kozma (1993).

Recently, using a time-dependent model of the hydrogen ionization with the kinetics of atomic and molecular hydrogen we have found that time-dependent effects in SN 1987A were strong during the first month and that they could provide the hydrogen excitation required to account for the $H\alpha$ line strength (Utrobin & Chugai 2002) which was underproduced in steady-state models of SN 1987A atmosphere. However, our previous

model has ignored a time-dependent energy balance; instead simple laws have been used to mimic the evolution of the electron temperature in the atmosphere.

Keeping in mind the importance of the non-steady state ionization effects for the understanding of the phenomena seen in early SN 1987A, we revisit this issue. To this end we upgrade the atmosphere model that apart from the time-dependent kinetics includes also the time-dependent energy balance. Our main goal is to compute the ionization and excitation of hydrogen in the atmosphere of SN 1987A for different epochs, and to compare the calculated $H\alpha$ line with the observations. We also address a highly intriguing problem of tremendous Ba overabundance that has been recovered by several studies (Mazzali et al. 1992; and references there). Our preliminary guess was that the Ba overabundance problem was caused by the strong underestimation of the Ba II ionization fraction.

We begin with a question, why time-dependent effects are important (Sect. 2) and then describe in detail the proposed model (Sect. 3). The $H\alpha$ strength on day 4.64 is used to constrain the kinetic energy of the hydrodynamic model Sect. 4.1, the computations of the ionization and temperature structure of the atmosphere along with the $H\alpha$ profiles for selected phases are presented in Sect. 4.2, while in Sect. 4.3 we address the problem of high Ba overabundance.

We adopt here the radial velocity of SN 1987A of 286.5 km s^{-1} (Meaburn et al. 1995) and the distance of 50 kpc.

2. Why time-dependent?

A widely shared view that the steady-state statistical equilibrium is a reasonable approximation for SN IIP atmospheres relies on the claim that the recombination time is much smaller than the SN age

$$(\alpha N_e)^{-1} \ll t, \quad (1)$$

where α is the coefficient of recombination to the excited states, N_e is the electron number density. Adopting $\alpha \sim 3 \times 10^{-13} \text{ cm}^3 \text{ s}^{-1}$ and a typical SN age at the photospheric epoch $t \sim 10^6 - 10^7 \text{ s}$ one finds that the requirement (1) is satisfied for $N_e \gg 10^7 \text{ cm}^{-3}$. This condition is actually met at the photosphere thus supporting the steady-state approximation. Meanwhile, it is violated in the outer, high velocity layers, where N_e may drop as low as 10^7 cm^{-3} . Therefore, generally, the time dependent approach is needed at least, if one addresses the situation in the outer layers.

Moreover, it turns out that the steady-state approximation is violated also in the inner atmosphere, where the condition (1) holds. The point is that this inequality has little in common with the condition of the steady state for multilevel atom irradiated by the optical continuum, because of the efficient reionization of recombined atom. The importance of this phenomenon has been first recognized for the problem of the hydrogen recombination in the early universe, where $L\alpha$ trapping along with the reionization from the second level results in the significant increase of the recombination time $t_{\text{rec}} = -N_e/(dN_e/dt)$ (Zeldovich et al. 1968).

The net recombination rate dN_e/dt refers to transitions to the ground state that either do not emit $L\alpha$ or followed by the escape of the emitted $L\alpha$ quantum without resonance scattering. Let the probability of such a transition is w_{21} . Then in the "two level plus continuum" approximation the net recombination rate (neglecting the expansion effect) is

$$\frac{dN_e}{dt} = -\alpha N_e^2 w_{21}. \quad (2)$$

With all the major processes from the second level taken into account the probability w_{21} is

$$w_{21} = \frac{A_{2q} + N_e q_{21} + A_{21} \beta_{21}}{P_2 + A_{2q} + N_e q_{21} + A_{21} \beta_{21}}, \quad (3)$$

where P_2 is the photoionization rate from the second level; A_{2q} is the probability of the two-photon decay evaluated for the equipartition of 2s and 2p levels; q_{21} is the collisional deexcitation coefficient; $A_{21} \beta_{21}$ is the $L\alpha$ escape probability.

Let us estimate w_{21} for the neutral hydrogen number density $N_1 > 10^9 \text{ cm}^{-3}$ and the electron number density $N_e < 10^8 \text{ cm}^{-3}$, when the two-photon transition dominates over collisional transition and $L\alpha$ escape, i.e., $w_{21} \approx A_{2q}/P_2$. This situation is typical for the inner atmosphere of SN IIP. With the photospheric temperature of $T \approx 5000 \text{ K}$ one gets $P_2 \approx 10^4 W \text{ s}^{-1}$, where W is the dilution factor. Close to the photosphere (for $W > 0.1$) one finds $w_{21} < 2 \times 10^{-3}$. The effective recombination time is then

$$t_{\text{rec}} = -N_e/(dN_e/dt) = 1/(\alpha N_e w_{21}) \sim 500/(\alpha N_e). \quad (4)$$

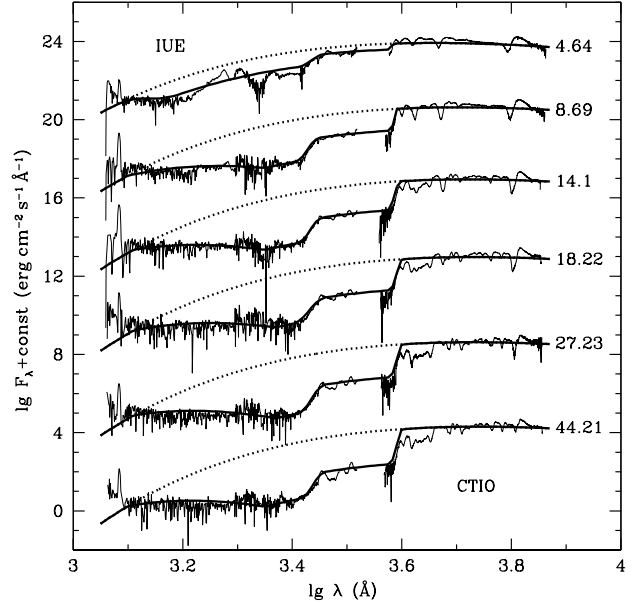


Fig. 1. The combined UV (IUE) (Pun et al. 1995) and optical (CTIO) (Phillips et al. 1988) spectra of SN 1987A (*thin solid line*), the black-body continuum at the calculated effective temperature of the high-energy model (*dotted line*), and the observed continuum (*thick solid line*) between days 4.64 and 44.21.

This shows that the effective recombination time is by a factor of $1/w_{21} \sim 500$ greater than the recombination time to excited states $1/(\alpha N_e)$. For $N_e \sim 10^8 \text{ cm}^{-3}$ one obtains $t_{\text{rec}} > 10^7 \text{ s} > t$. We thus conclude that the steady-state approximation may break down in the dense inner atmosphere as well.

These qualitative considerations demonstrate that the hydrogen recombination in the atmosphere of SN IIP at the photospheric epoch is essentially a time-dependent phenomenon.

3. The model and input physics

A self-consistent treatment of the SN atmosphere requires the hydrodynamic modelling with time-dependent radiation transport, energy balance, and ionization kinetics. At present such a general approach is beyond reach of computation possibilities. To study time-dependent effects in the atmosphere of SN 1987A and yet to make the problem solvable, we sacrifice the radiation transfer in the atmosphere using, instead, a simple description of the continuum radiation field.

3.1. Continuum radiation

The SN atmosphere is very opaque in the Lyman continuum ($\nu > \nu_1$), so the photoionization by the photospheric Lyman continuum can be neglected. On the other hand, the hydrogen ionization by the recombination Lyman continuum in the atmosphere can be easily taken into account via cancelling the photoionization of hydrogen from the ground level and the recombination to the ground level in the rate equations. In the at-

mosphere the radiation field in continuum at these frequencies is considered as being in the thermal equilibrium with matter.

The important simplification we adopt is that the continuum in the range of $\nu < \nu_1$ corresponds to the free-streaming case, i.e., the average intensity of the continuum in the atmosphere is $J_\nu = WI_\nu$, where I_ν is the specific intensity of the photospheric radiation. The photospheric radius R_{ph} and effective temperature T_{eff} are provided by the hydrodynamic model.

The free-streaming approximation is a good approximation in the visual band, where the optical depth of the atmosphere is quite low. However, for the ultraviolet (UV) radiation between Lyman and Balmer edges this approximation is indeed rather artificial, because of the large optical depth due to the UV line opacity. As a result, the average intensity of the UV radiation in the atmosphere generally should differ from the free-streaming approximation.

Nevertheless, this approximation is not as bad as one would think at first glance. It predicts behavior of $J \propto r^{-2}$ in the most of the atmosphere. In the case of pure scattering with the constant scattering coefficient ($\chi(r) = \text{const}$) one obtains for the extended atmosphere $J \propto [1 + 1.5R\chi(R/r - 1)]$ where R is the outer radius of the atmosphere (Chandrasekhar 1934). According to this expression the behavior of $J(r)$ is steeper than r^{-2} for outer layers ($r \sim R$) and $J(r) \propto r^{-1}$ for $r \ll R$. So, our approximation corresponds to some intermediate range in the atmosphere. Moreover, since the scattering of UV metal lines is liable to photon splitting, the interaction of the UV radiation with matter will be close to the absorption rather than scattering. We expect, therefore, more steep behavior of $J(r)$ in the inner layer compared to the pure scattering case. In that case the law $J \propto r^{-2}$ may be a sensible approximation in the deeper layers as well.

To further allow for the uncertainty of our approximation we consider two extreme cases: (i) the photospheric brightness is black-body with the effective temperature (model A); (ii) the photospheric brightness corresponds to the observed spectrum (model B) (Fig. 1). The real situation is somewhere between these two cases.

3.2. Hydrodynamic model

The density distribution, chemical composition, radius of the photosphere and effective temperature are provided by the hydrodynamic model of SN 1987A (see for details Utrobin 2004). We consider the non-evolutionary model N of Utrobin (2004) with $18 M_\odot$ ejecta, kinetic energy of 10^{51} erg, and ^{56}Ni mass of $0.073 M_\odot$. For the distance modulus to the LMC of $m - M = 18.5$ mag, color excess of $E(B - V) = 0.15$ mag, and an interstellar extinction of $A_V = 3.1E(B - V)$ mag a progenitor of SN 1987A, Sanduleak $-69^\circ 202$, had the radius of $46.8 R_\odot$. To produce the presupernova density distribution the evolutionary model I20n2ae of Woosley et al. (1997) was rescaled to adopted radius and ejecta mass. We assumed for the outer layers the circumstellar helium abundance $Y = 0.441$ (Wang 1991; Lundqvist & Fransson 1996) and the LMC metallicity $Z = 0.004$ (Dufour 1984). The structure of the presupernova outer layers was modified to increase density compared with

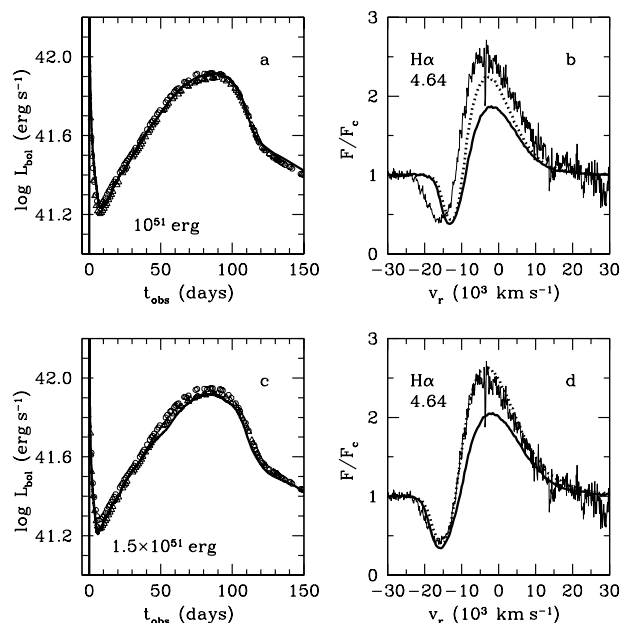


Fig. 2. Comparison of the low and high-energy models of SN 1987A. Top: (a) bolometric light curve of the low-energy model (*thick solid line*) compared with the observations of SN 1987A obtained by Catchpole et al. (1987, 1988) (*open circles*) and Hamuy et al. (1988) (*open triangles*), and (b) the $H\alpha$ line profile on day 4.64 computed on the basis of this hydrodynamic model for the black-body continuum (model A) (*dotted line*) and the observed continuum (model B) (*thick solid line*). The calculated spectra are overplotted on the observed spectrum (Phillips et al. 1988) (*thin solid line*). Bottom: (c) bolometric light curve of the high-energy model and (d) the corresponding $H\alpha$ profile on day 4.64.

the evolutionary model of non-rotating single star. This correction was needed to fit the observed bolometric light curve of SN 1987A (Fig. 2a) with a moderate mixing of radioactive ^{56}Ni in the velocity range $\leq 2500 \text{ km s}^{-1}$ (Utrobin 2004). The final model is dubbed as the low-energy model.

We consider also the high-energy version of the above model. This model with the kinetic energy 1.5×10^{51} erg differs from the low-energy model by the presupernova radius of $35.0 R_\odot$, ^{56}Ni mass of $0.075 M_\odot$, and the adopted color excess of $E(B - V) = 0.17$ mag (Michael et al. 2003). The chemical composition of the outer layers is typical to the LMC chemical composition, $X = 0.743$, $Y = 0.251$, and $Z = 0.006$ (Dufour 1984). This model agrees with the observed bolometric light curve of SN 1987A for ^{56}Ni mixed in the velocity range $\leq 3000 \text{ km s}^{-1}$ (Fig. 2c).

3.3. Line transfer

Starting the first day the envelope of SN 1987A expands homologously (Utrobin 2004), so the Sobolev approximation is

applicable. In this approximation the line transfer is described by the escape probability (Sobolev 1960; Castor 1970)

$$\beta_{lu} = \frac{1 - \exp(-\tau_{lu})}{\tau_{lu}}, \quad (5)$$

where

$$\tau_{lu} = \frac{\pi e^2}{m_e c} f_{lu} \lambda_{lu} t \left(N_l - \frac{g_l}{g_u} N_u \right) \quad (6)$$

is the Sobolev optical depth in a transition from level l to level u . Here N_l , g_l , N_u , g_u are number densities and statistical weights of atoms in the lower and upper levels, respectively, f_{lu} is the oscillator strength, and λ_{lu} is the line wavelength. In the Sobolev approximation the frequency-averaged mean intensity of the line is

$$J_{lu} = (1 - \beta_{lu}) S_{lu} + \beta_{lu} J(\nu_{lu}), \quad (7)$$

where

$$S_{lu} = \frac{2h\nu_{lu}^3}{c^2} \left(\frac{g_u N_l}{g_l N_u} - 1 \right)^{-1} \quad (8)$$

is the line source function and ν_{lu} is the line frequency. The net frequency-integrated line emissivity is

$$\eta_{ul} = \frac{1}{4\pi} h\nu_{lu} N_u A_{ul} \beta_{ul} \left(1 - \frac{J(\nu_{lu})}{S_{lu}} \right), \quad (9)$$

where A_{ul} is the Einstein spontaneous emission probability for the transition from level u to level l .

For the very opaque $L\alpha$ line the Sobolev approximation is violated, if one consider the $L\alpha$ radiation transfer, but remains valid, if one is interested in the computations of the escape rate (Chugai 1980).

3.4. Gamma-rays and positrons deposition

The gamma rays with energy of about 1 MeV from the decay chain $^{56}\text{Ni} \rightarrow ^{56}\text{Co} \rightarrow ^{56}\text{Fe}$ deposit their energy through Compton scattering by free and bound electrons. The Compton electrons lose their energy through the Coulomb heating of free electrons and the ionization and excitation of atoms and ions. The rates of the heating, non-thermal ionization and excitation for atoms and ions are taken according to Kozma & Fransson (1992). The gamma-rays transport is calculated in the approximation of the effective absorption opacity of $0.06 Y_e \text{ cm}^2 \text{ g}^{-1}$, where Y_e is the number of electrons per baryon. Positrons are assumed to deposit their energy locally.

3.5. Rate equations

The following elements and molecules are calculated in time-dependent non-LTE chemical kinetics: H, He, C, N, O, Ne, Na, Mg, Si, S, Ar, Ca, Fe, Ba, H^- , H_2 , H_2^+ , and H_3^+ . All elements but H are treated with the three ionization stages. Neutral hydrogen and ions Mg II, Fe II, and Ba II are modelled with 15, 9, 30, and 17 levels, respectively, while other atoms and ions are assumed to consist of the ground state and continuum. The reaction network includes all bound-bound and bound-free, radiative and

collisional processes for the atoms and ions with a detailed level structure (Appendices A.1–A.4), all bound-free, radiative and collisional processes for the two-state atoms and ions (Appendix A.5). We consider kinetics of hydrogen molecules that may affect the hydrogen ionization degree. Seven radiative and 37 collisional processes for the molecules are taken into account (Appendices B.1–B.2).

For one-dimensional, spherically symmetric flow the equation of continuity simplifies to

$$\frac{\partial \rho}{\partial t} = -\frac{\rho}{t_{exp}}, \quad \frac{1}{t_{exp}} = \left(2 + \frac{\partial \ln v}{\partial \ln r} \right) \frac{v}{r}, \quad (10)$$

where $\partial/\partial t$ is the Lagrangean time derivative; ρ is the density of the matter; r and v are radius and velocity, respectively. The net rate of transitions between level k and all other levels of neutral atom z by atomic processes is

$$\begin{aligned} \left[\frac{\partial N_{z^0,k}}{\partial t} \right] &= \sum_{u>k} N_{z^0,u} A_{uk} \left(1 - \frac{J_{lu}}{S_{ku}} \right) + N_{z^+} N_e \alpha_k \\ &- N_{z^0,k} \sum_{l<k} A_{kl} \left(1 - \frac{J_{lu}}{S_{lk}} \right) - N_{z^0,k} P_k \\ &+ N_e \sum_{u>k} (N_{z^0,u} q_{uk} - N_{z^0,k} q_{ku}) + N_{z^+} N_e^2 q_{c,k} \\ &- N_e \sum_{l<k} (N_{z^0,k} q_{kl} - N_{z^0,l} q_{lk}) - N_e N_{z^0,k} q_{k,c} \\ &+ R_k^\gamma - R_{k,c}^\gamma, \end{aligned} \quad (11)$$

where $N_{z^0,k}$ is the number density of neutral atom z at the level k ; N_{z^+} is the number density of singly ionized element z ; N_e is the number density of free electrons; J_{lu} is the frequency-averaged mean intensity of the line (7); S_{lu} is the line source function (8); α_k and P_k are the total radiative recombination coefficient, including the spontaneous and induced processes, and the photoionization rate of neutral atom z in level k , respectively (Mihalas 1978); q_{lu} is the electron collisional excitation rate from level l to level u ; $q_{ul} = (N_{z^0,l}/N_{z^0,u})^* q_{lu}$ is the corresponding deexcitation rate and the ratio $(N_{z^0,l}/N_{z^0,u})^*$ for the local thermodynamic equilibrium (LTE) is given by the Boltzmann formula; $q_{k,c}$ is the electron collisional ionization rate from level k ; $q_{c,k} = (N_{z^0,k}/N_{z^+} N_e)^* q_{k,c}$ is the corresponding recombination coefficient and the LTE ratio $(N_{z^0,k}/N_{z^+} N_e)^*$ is given by the Saha equation; R_k^γ and $R_{k,c}^\gamma$ are the non-thermal excitation and ionization rates of neutral atom z in level k , respectively (Kozma & Fransson 1992).

The rate equation for the number density $N_{\text{H}^0,2}$ of neutral hydrogen in level 2 is determined by the net rate of flow of particles into the unit volume with a characteristic time t_{exp} (10), the net rate (11), hydrogen two-photon decays, and other depopulation processes:

$$\begin{aligned} \frac{\partial N_{\text{H}^0,2}}{\partial t} &= -\frac{N_{\text{H}^0,2}}{t_{exp}} + \left[\frac{\partial N_{\text{H}^0,2}}{\partial t} \right] - A_{2s,1s}^{2q} N_{\text{H}^0,2s} \\ &- k_5 N_{\text{H}^0} N_{\text{H}^0,2s} - k_6 N_{\text{H}^0} N_{\text{H}^0,2p} \\ &- k_8 N_{\text{H}^0,1} N_{\text{H}^0,2s} - k_9 N_{\text{H}^0,1} N_{\text{H}^0,2p} \\ &- k_{14} N_{\text{H}_2} N_{\text{H}^0,2}, \end{aligned} \quad (12)$$

where $N_{\text{H}^0,2s} = 0.25 N_{\text{H}^0,2}$ and $N_{\text{H}^0,2p} = 0.75 N_{\text{H}^0,2}$ are the number density of hydrogen levels 2s and 2p calculated assuming

only collisional transition between these states; $N_{\text{H}^0} = \sum_{k=1}^{15} N_{\text{H}^0,k}$ is the number density of neutral hydrogen; N_{H_2} is the number density of H_2 ; $A_{2s,1s}^{2q}$ is the probability of the hydrogen two-photon decay; k_5, k_6, k_8, k_9 , and k_{14} are the rate coefficients for the corresponding reactions from Table B.1. The rate equations for the number density of neutral hydrogen in level 3 and higher levels $k > 3$ are

$$\frac{\partial N_{\text{H}^0,3}}{\partial t} = -\frac{N_{\text{H}^0,3}}{t_{\text{exp}}} + \left[\frac{\partial N_{\text{H}^0,3}}{\partial t} \right] - k_7 N_{\text{H}^0} N_{\text{H}^0,3} - k_{14} N_{\text{H}_2} N_{\text{H}^0,3} \quad (13)$$

and

$$\frac{\partial N_{\text{H}^0,k}}{\partial t} = -\frac{N_{\text{H}^0,k}}{t_{\text{exp}}} + \left[\frac{\partial N_{\text{H}^0,k}}{\partial t} \right] - k_{14} N_{\text{H}_2} N_{\text{H}^0,k}, \quad (14)$$

respectively. Similarly, the rate equation for the number density $N_{z^+,k}$ of ions $z^+ = \text{Mg}^+, \text{Fe}^+, \text{Ba}^+$ in level k simply is

$$\frac{\partial N_{z^+,k}}{\partial t} = -\frac{N_{z^+,k}}{t_{\text{exp}}} + \left[\frac{\partial N_{z^+,k}}{\partial t} \right]. \quad (15)$$

The rate equations for ionized hydrogen, negative hydrogen ion, and molecular hydrogen H_2 , H_2^+ and H_3^+ are given in Appendix C.

For the two-state atoms and ions the net rate of transitions, for example, from neutral atom z into ion z^+ by ionization and recombination processes is given by

$$\left[\frac{\partial N_{z^+}}{\partial t} \right] = N_{z^0} (P_{z^0} + N_e q_{z^0,c} + R_{z^0,c}^y) - N_{z^+} N_e (\alpha_{z^0} + N_e q_{c,z^0}). \quad (16)$$

Using the net rate (16) the rate equations for elements with three ionization stages are easily generalized:

$$\frac{\partial N_{z^+}}{\partial t} = -\frac{N_{z^+}}{t_{\text{exp}}} + \left[\frac{\partial N_{z^+}}{\partial t} \right] - \left[\frac{\partial N_{z^{2+}}}{\partial t} \right] \quad (17)$$

and

$$\frac{\partial N_{z^{2+}}}{\partial t} = -\frac{N_{z^{2+}}}{t_{\text{exp}}} + \left[\frac{\partial N_{z^{2+}}}{\partial t} \right]. \quad (18)$$

In particular, the rate equation for singly ionized oxygen taking account of the charge transfer processes in collisions of H^+ with O and O^+ with H is

$$\frac{\partial N_{\text{O}^+}}{\partial t} = -\frac{N_{\text{O}^+}}{t_{\text{exp}}} + \left[\frac{\partial N_{\text{O}^+}}{\partial t} \right] - \left[\frac{\partial N_{\text{O}^{2+}}}{\partial t} \right] + k_{\text{HO}} N_{\text{H}^+} N_{\text{O}^0} - k_{\text{OH}} N_{\text{O}^+} N_{\text{H}^0}, \quad (19)$$

where N_{H^+} is the number density of ionized hydrogen. The net rate (16) for the ions with a detailed level structure (Mg^+, Fe^+ , and Ba^+) is calculated including all relevant atomic processes.

To close the system of the above rate equations (12–15, C.1–C.5, 17–19) we use the particle conservation for hydrogen

$$N_{\text{H}^0} + N_{\text{H}^+} + N_{\text{H}^-} + 2N_{\text{H}_2} + 2N_{\text{H}_2^+} + 3N_{\text{H}_3^+} = \frac{\rho X_{\text{H}}}{m_u A_{\text{H}}} \quad (20)$$

and for other elements from He to Ba with three ionization stages

$$N_{z^0} + N_{z^+} + N_{z^{2+}} = \frac{\rho X_z}{m_u A_z}, \quad (21)$$

and the charge conservation

$$N_{\text{H}^+} - N_{\text{H}^-} + N_{\text{H}_2^+} + N_{\text{H}_3^+} + \sum_{z=\text{He}}^{\text{Ba}} (N_{z^+} + 2N_{z^{2+}}) = N_e, \quad (22)$$

where X_z is the mass fraction of element z , and A_z is its atomic weight.

3.6. Gas energy equation

The equation of state of a perfect gas can be written as

$$P_g = (N_t + N_e) k T_e, \quad (23)$$

where P_g is gas pressure and N_t is the total number density of atoms, molecules, and ions of all types. The specific internal energy of particles (per gram) is the sum of the translational, excitation, and ionization energies:

$$E_g = \frac{3}{2} \frac{N_t + N_e}{\rho} k T_e + E_{\text{exc}} + E_{\text{ion}}, \quad (24)$$

where

$$E_{\text{exc}} = \sum_{z=\text{H}}^{\text{Ba}^+} \sum_{k>1} \epsilon_{z,k} N_{z,k} \quad (25)$$

is the excitation energy and

$$E_{\text{ion}} = I_{\text{H}} N_{\text{H}^+} - I_{\text{H}^-} N_{\text{H}^-} + I_{\text{H}_2} N_{\text{H}_2^+} + I_{\text{H}_3} N_{\text{H}_3^+} + \sum_{z=\text{He}}^{\text{Ba}} [I_{z^0} N_{z^0} + (I_{z^+} + I_{z^{2+}}) N_{z^{2+}}], \quad (26)$$

is the ionization energy. Here $\epsilon_{z,k}$ is the excitation energy of state k for the corresponding atoms and ions, and $I_{\text{H}}, I_{\text{H}^-}, I_{\text{H}_2}, I_{\text{H}_3}, I_{z^0}, I_{z^+}$ are the ionization potentials of the corresponding atoms, molecules, and ions.

The gas energy equation, the first law of thermodynamics for the material, including radiative losses in continuum and lines, the Compton cooling, and non-thermal heating thus reads

$$\frac{\partial E_g}{\partial t} + P_g \frac{\partial}{\partial t} \left(\frac{1}{\rho} \right) = \frac{4\pi}{\rho} \int_0^\infty (\kappa_\nu J_\nu - \eta'_\nu - \eta_\nu^{2q}) d\nu - \frac{4\pi}{\rho} \left(\sum_{z=\text{H}}^{\text{Ba}^+} \sum_{l,u} \eta_{ul} + \eta^{\text{C}} \right) + \mathcal{E}^y, \quad (27)$$

where

$$\eta^{\text{C}} = \frac{4kT_e}{m_e c^2} \sigma_e N_e J \left(1 - \frac{T_r}{T_e} \right) \quad (28)$$

is the net emissivity of the Compton cooling (Weymann 1966). Here κ_ν and η'_ν are the monochromatic true absorption coefficient corrected for stimulated emission and the monochromatic thermal emissivity, including bound-free and free-free processes for all atoms and ions, respectively (Mihalas 1978);

η_v^{2q} is the two-photon emissivity of hydrogen; η_{ul} is the net frequency-averaged emissivity of line (9); ε^γ is the rate of energy deposition from the radioactive decays; σ_e is the Thomson scattering cross section; J is the integrated mean intensity of continuum; $T_r = (\pi J / \sigma_R)^{1/4}$ is the radiation temperature and σ_R is the Stefan-Boltzmann constant. The energy equation determines the electron temperature in the SN atmosphere which is the same for neutrals and ions.

3.7. Computational method

A hydrodynamic model with 300 mass zones provides us the velocity $v(r, t)$ and density $\rho(r, t)$ profiles, the photospheric radius $R_{ph}(t)$ and effective temperature $T_{eff}(t)$. The simplified description of the continuum radiation field as diluted photospheric radiation permits us to solve for a given mass zone the rate equations (12–15, C.1–C.5, 17–19), the particle conservation equations (20, 21), the charge conservation equation (22), and the gas energy equation (27) independently of other mass zones.

As the supernova envelope expands the photosphere moves inward the envelope. In a steady state the physical values in the atmosphere at certain moment t are determined by the instant density and radiation field. In a time-dependent approach one has to start from a moment t_{ph} at which a given mass zone crosses the photosphere, and then to follow the time evolution until t . To obtain the distribution of physical values in the atmosphere this procedure should be applied to each mass zone.

The simultaneous solution of the above equations (12–14, C.1–C.5, 17–22, 27) is achieved by reducing them to a system of ordinary differential equations. In particular, the gas energy equation (27) is reduced to the ordinary differential equation for electron temperature T_e . To properly formulate the problem of time evolution of physical values for a given mass zone, initial data must be specified at the photospheric level. This is done by solving the equations (12–14, C.1–C.5, 17–22) at the photospheric level assuming the steady state for a given electron temperature T_e . This is the simplest way to model the non-equilibrium conditions at the SN photosphere. The derived system of ordinary differential equations is stiff and is integrated by the implicit method of Gear (1971) with an automatic choice of both the time integration step and the order of accuracy of the method.

The recovered time-dependent structure of the atmosphere is used then to calculate spectra at selected epochs. The spectra are modelled by Monte Carlo technique with relativistic effects included (Mihalas 1978; Jeffery 1993, 1995). We suggest that the photosphere diffusively reflects the incident photons (Chugai & Utrobin 2000). The line scattering is generally non-conservative and is described in terms of the line scattering albedo. The Thomson scattering on free electrons and Rayleigh scattering on neutral hydrogen are taken into account.

4. Results

4.1. Early $H\alpha$ and the hydrodynamic model

Preliminary modelling of $H\alpha$ has revealed that at the early epoch the $H\alpha$ line strength was sensitive to the density of the outer layers. A similar sensitivity of the $H\alpha$ strength to the density was found in the steady-state model (Eastman & Kirshner 1989). We use therefore the $H\alpha$ on day 4.64 to constrain the kinetic energy of the hydrodynamic model.

Assuming the initial electron temperature equal to the effective temperature $T_e = T_{eff}$ we solved the system of rate and energy equations and then computed $H\alpha$ profile for the low-energy model, i.e., for the model N with the kinetic energy $E = 10^{51}$ erg (Utrobin 2004). The corresponding bolometric light curve and the calculated $H\alpha$ profile on day 4.64 are shown in Figs. 2a and 2b. The computed $H\alpha$ line has too weak absorption at high velocities compared to the observations (Phillips et al. 1988). The situation, however, is markedly improved for the high-energy model with $E = 1.5 \times 10^{51}$ erg (Figs. 2c and 2d). The larger strength of the $H\alpha$ absorption in the high-energy model is the direct outcome of the higher density in the outer layers. Thus, the strength of the $H\alpha$ absorption at high velocities indicates the favoring energy-to-mass ratio $E/M \approx 0.83 \times 10^{50} \text{ erg } M_\odot^{-1}$. We adopt the model with the high energy as the standard model for our computations of the SN 1987A atmosphere.

4.2. Evolution of hydrogen ionization and $H\alpha$

With the adopted photospheric continuum and the initial electron temperature we are able to compute for given moments the distribution of the essential physical values in the atmosphere, including the hydrogen level populations. The initial electron temperature at the photosphere is adopted equal to the effective temperature T_{eff} which is taken from the hydrodynamical calculations (Utrobin 2004).

4.2.1. Day 4.64

On day 4.64 the $H\alpha$ profile computed in the time-dependent model A fits the observed one fairly well (Fig. 3a), while the model B underproduces the emission component (Fig. 3b). This suggests that the average intensity of the UV radiation in the atmosphere at this and earlier epochs is closer to that of the model A. The steady-state model A produces rather strong $H\alpha$ line although both the absorption and emission components are markedly weaker than in the observed line, while in the steady-state model B the $H\alpha$ line is extremely weak. The weakness of the $H\alpha$ line in the steady-state model reflects the simple fact that the steady-state ionization is lower than that in the time-dependent model.

As expected, the electron temperature in the model A is larger than in the model B since the radiative heating rate in the model A with the black-body UV continuum is higher than in the model B (Figs. 3c and 3d). The remarkable property of the distribution of electron temperature in the atmosphere for both models is a fast drop from the initial value at the photosphere of

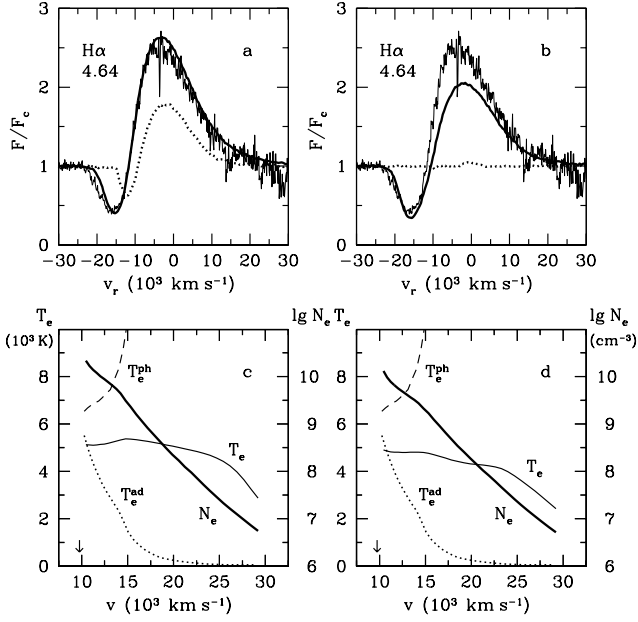


Fig. 3. $H\alpha$ line profile and the structure of the atmosphere on day 4.64. Panel (a): $H\alpha$ profile computed with the time-dependent model A (*thick solid line*) and with the steady-state model A (*dotted line*), and overplotted on the observed profile obtained by Phillips et al. (1988) (*thin solid line*). Panel (b): the same as panel (a) but for the model B. Panel (c): the calculated electron number density (*thick solid line*) and electron temperature (*thin solid line*) in the time dependent model A. The *dashed line* shows the initial electron temperature T_e^{ph} at the photosphere as a function of velocity, while the *dotted line* is the distribution of the electron temperature T_e^{ad} evaluated with the purely adiabatic cooling. Arrow indicates the photospheric level. Panel (d): the same as panel (c) but for the model B.

T_{eff} to $\sim (0.75\text{--}0.80) T_{\text{eff}}$. This drop results from a simple fact that the electron temperature calculated in the diluted radiation field is lower than the effective temperature. The same physics leads to a well known relation for the boundary temperature of gray atmosphere $T_0 \approx 0.81 T_{\text{eff}}$ (see, e.g., Mihalas 1978).

Although the electron temperature is relatively high in the most of the atmosphere, $T_e > 4000$ K, (Figs. 3c and 3d) it is insufficient to maintain the large optical depth of $H\alpha$ demonstrated by the time-dependent models. The primary mechanism of the population of the second level is the recombination to excited levels.

Noteworthy, the populations of excited levels are small numbers that are controlled by the relatively fast transition rates. As a result the relaxation times for the level populations of hydrogen are small: $N_{\text{H}^0,k}/(dN_{\text{H}^0,k}/dt) \ll t$. So the populations of excited levels may be considered in the steady-state approximation. We conclude that the population of the second hydrogen level, and the $H\alpha$ optical depth as well, is determined mainly by the current values of the electron concentration and the photoionization rates, which are essentially time-dependent.

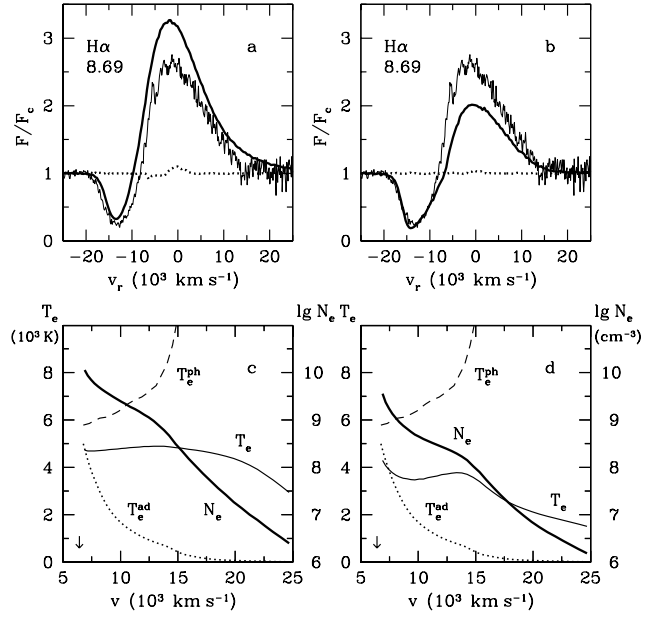


Fig. 4. $H\alpha$ line profile and the structure of the atmosphere on day 8.69. See Fig. 3 legend for details.

4.2.2. Day 8.69

On day 8.69 the both A and B models reproduce satisfactorily the absorption component of $H\alpha$ (Figs. 4a and 4b). The strength of observed emission lies between two models which implies that the actual radiation field in the UV band is intermediate between A and B cases. The steady-state approach in both models predicts very weak $H\alpha$ line at this epoch. This is qualitatively consistent with the steady-state modelling of Mitchell et al. (2002).

The electron concentration shows a kink at about 14000 km s^{-1} (Figs. 4c and 4d) that was only barely seen at the previous date (Figs. 3c and 3d). The position of this kink correlates with the transition from the full ionization to partial ionization at the photosphere that occurred after $t \approx 2$ days.

4.2.3. Day 14.68 and 19.68

The calculated $H\alpha$ profiles on day 14.68 (Figs. 5a and 5b) and 19.68 (Figs. 6a and 6b) show similar behavior. The model B fits to the observed profile fairly well, whereas the emission component in the model A is unacceptably strong. This indicates that around these epochs the UV continuum radiation is closer to that of the model B. The steady-state model at this phase is very weak with practically zero absorption and emission components.

At these epochs the adiabatic cooling in the model B dominates at the low velocities as indicated by the close run of temperatures T_e and T_e^{ad} (Figs. 5d and 6d), and the most of the atmosphere is cooled below ~ 2000 K. In the model A the heating due to the photoionization is strong enough to maintain rather high temperature ~ 4000 K throughout the atmosphere.

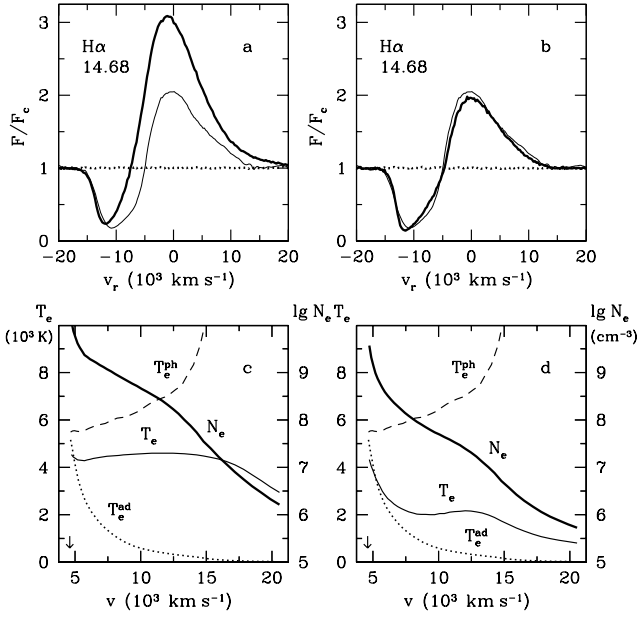


Fig. 5. $H\alpha$ line profile and the structure of the atmosphere on day 14.68. Observed profile is given by Hanuschik & Dachs (1988). See Fig. 3 legend for details.

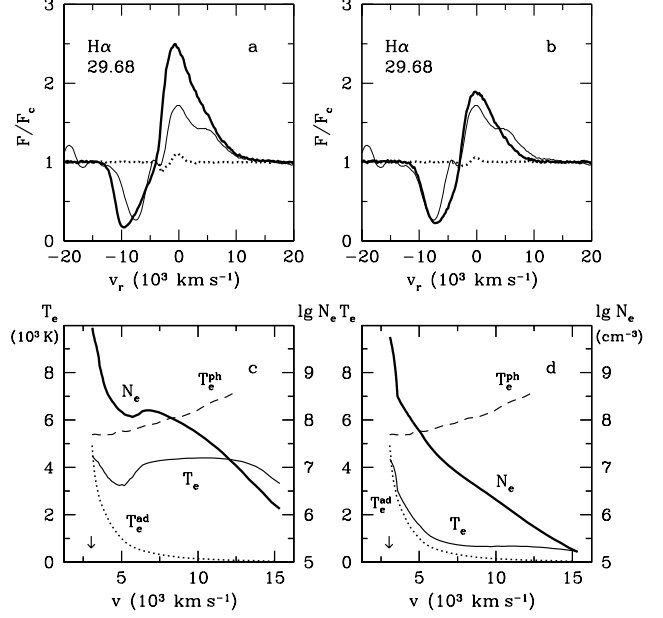


Fig. 7. $H\alpha$ line profile and the structure of the atmosphere on day 29.68. Observed profile is given by Hanuschik & Dachs (1988). See Fig. 3 legend for details.

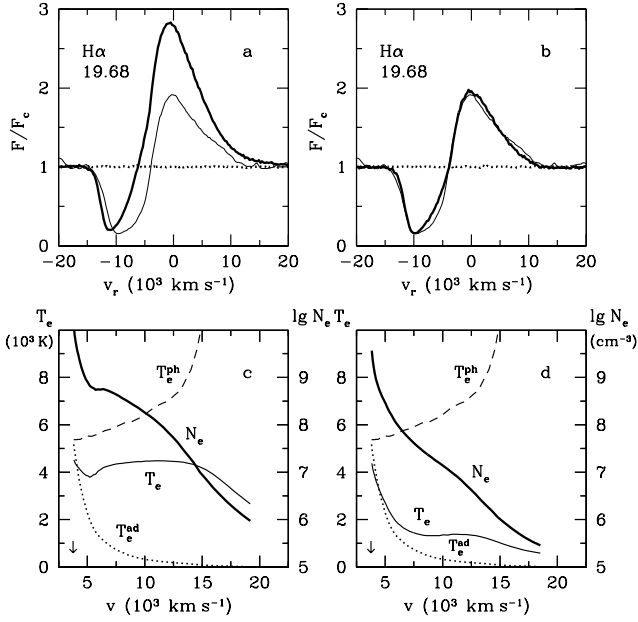


Fig. 6. $H\alpha$ line profile and the structure of the atmosphere on day 19.68. Observed profile is given by Hanuschik & Dachs (1988). See Fig. 3 legend for details.

4.2.4. Day 29.68

On day 29.68 the model A leads to the unacceptably strong $H\alpha$ emission (Fig. 7a), while the model B reproduces the overall strength of the absorption and emission components of $H\alpha$ (Fig. 7b). The $H\alpha$ line in the steady-state models is extremely weak, although slightly stronger than on day 14.68 and 19.68.

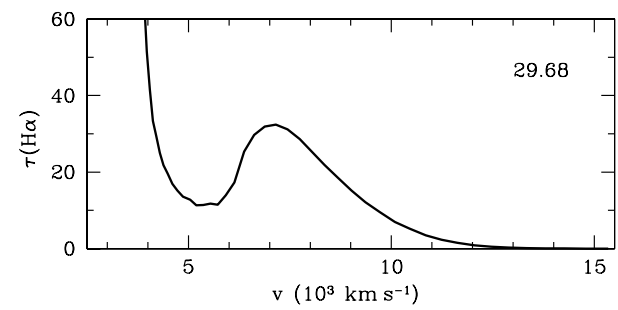


Fig. 8. The $H\alpha$ optical depth on day 29.68 in the model A. The local minimum at 5000 km s^{-1} is a characteristic feature required for the explanation of the blue peak.

The behavior of electron temperature T_e and electron concentration N_e is very different for both models (Figs. 7c and 7d) that emphasizes the sensitivity of the result to the behavior of the UV radiation field in the atmosphere. Yet, it is highly remarkable that even the time-dependent model B, in which the UV continuum intensity is possibly underestimated, reproduces the strength of the $H\alpha$ line in the whole range of the radial velocities. This means that the admixed ^{56}Ni in the outer layers is not needed to account for the $H\alpha$ line in SN 1987A at the age of $t \leq 30$ days.

Between day 20 and 29 the additional blue and red peaks emerge in $H\alpha$ profile, a phenomenon known as "Bochum event" (Hanuschik & Dachs 1988). We believe that the red peak is related with the high velocity ^{56}Ni clump in the far hemisphere, whereas the blue peak reflects a minimum in the spherically-symmetric radial distribution of the $H\alpha$ optical

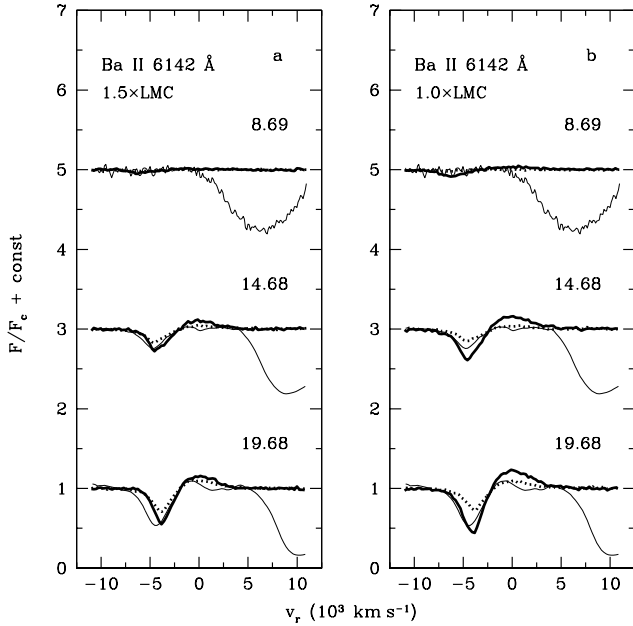


Fig. 9. Evolution of Ba II 6142 Å line from day 8.69 till 19.68 in SN 1987A. The Ba II 6142 Å profiles, computed with the time-dependent models A (*dotted line*) and B (*thick solid line*), are overlotted on those observed by Phillips et al. (1988) and Hanuschik & Dachs (1988) (*thin solid line*). Left panel (a): models for the relative Ba overabundance of 1.5. Right panel (b): models with the suppressed far UV continuum.

depth at $\approx 5000 \text{ km s}^{-1}$ (Chugai 1991b; Utrobin et al. 1995). The mechanism responsible for such a minimum is still not identified confidently. Both A and B models do not show any signature of the blue peak in $H\alpha$ profile. Remarkably, however, the model A reveals an essentially *non-monotonic* behavior of the $H\alpha$ optical depth $\tau(H\alpha)$ (Fig. 8) with the position of the minimum at 5000 km s^{-1} , just at the place that corresponds to the blue peak. Unfortunately, the optical depth at this minimum is too high to produce the blue peak in the $H\alpha$ profile. The required value should be 30 times lower. However the very possibility that the non-monotonic behavior of $\tau(v)$ may arise in a model with monotonic evolution of the photospheric parameters and monotonic density distribution is very promising for the explanation of the blue peak in the $H\alpha$ profile at the Bochum event phase.

Previously, using the time-dependent model we found that the enhanced hydrogen neutralization at about 4000 km s^{-1} governed by H^- and H_2^+ might be responsible for the local minimum of N_e and thus, for the minimum of the $H\alpha$ optical depth $\tau(H\alpha)$ (Utrobin & Chugai 2002). However, in that model we adopted rather simple behavior of electron temperature T_e in the atmosphere and at the photosphere. As a result the role of the molecular processes has been significantly exaggerated.

4.3. Barium problem

The “Ba problem” is the disparity between the high Ba overabundance factor $\zeta = (\text{Ba}/\text{Fe})_{87A}/(\text{Ba}/\text{Fe})_{\text{LMC}} \sim 5$ derived from Ba II 6142 Å line (Mazzali et al. 1992) and the theoretical predictions of *s*-process calculations. The *s*-process nucleosynthesis in the massive stars evolving to the presupernova star of SN 1987A (Prantzos et al. 1990) yields the Ba overabundance of $\zeta \sim 1.3\text{--}1.4$ in the hydrogen-rich envelope, assuming that a total ejecta mass is $15\text{--}18 M_{\odot}$, a mass-cut is at $2 M_{\odot}$ (Woosley & Weaver 1995), and the synthesized Ba is completely mixed over the ejecta. In fact, it is highly difficult to imagine that Ba produced at the He-burning stage can be significantly mixed with the hydrogen envelope. More realistic would be a situation with the LMC abundance of Ba in the hydrogen envelope.

In our time-dependent approach we recover the distribution of the electron concentration that fits to the $H\alpha$ profile on day 14.68 and 19.68 in the model B. Therefore we hope that our model can recover a more realistic abundance of Ba from Ba II 6142 Å line. We compute the Ba ionization and excitation, using the multilevel Ba II model described in Appendix A.4, for the two choices of the far UV ($10.0 < h\nu < 13.6 \text{ eV}$) radiation in the SN envelope. In the first version the continuum in this energy range is the diluted photospheric radiation — our standard assumption for models A and B (Fig. 1). In the second version we follow the suggestion of Mazzali et al. (1992) that the far UV continuum should be essentially suppressed by the line-blocking (in fact Rayleigh scattering also contributed to the blocking effect). This assumption essentially increases the ionization fraction of Ba II and thus decreases the overabundance factor. We, however, modify this assumption making it more realistic: we adopt that the far UV ($10.0 < h\nu < 13.6 \text{ eV}$) radiation is in equilibrium with matter and is characterized by the local electron temperature of our time-dependent model. This is the same approximation as accepted above for $h\nu > 13.6 \text{ eV}$. Unfortunately, the IUE observations cannot provide a confident verification of our assumption about the far UV flux in SN 1987A because of the dominant contribution of the light from the stars 2 and 3 to this band (Pun et al. 1995). We find that the accepted suppression of the far UV continuum does not affect the computed $H\alpha$ line for A and B cases at all.

The Ba II 6142 Å line profile calculated for three phases preceding the Bochum event are shown in Fig. 9. In the first version of the continuum the Ba relative abundance of $\zeta = 1.5$ is required to reproduce the Ba II 6142 Å line (Fig. 9a), while in the second case the LMC abundance of Ba ($\zeta = 1$) is quite enough (Fig. 9b). We find that for $\zeta = 5$ the blue wing of the line can be reproduced in the model B on day 14.68 and 19.68 with the photospheric far UV radiation. Note that Mazzali et al. (1992) obtained a similar overabundance in the model with the essentially suppressed far UV radiation. In our model with the suppressed far UV radiation the LMC abundance of Ba suffices to account for the Ba II 6142 Å line on day 14.68 and 19.68 (Fig. 9b). Note that in this case the model B produces too strong Ba II 6142 Å line on day 8.69, while the model A produces too weak line. This is consistent with our previous conclusion that at this epoch the $H\alpha$ line requires the intermediate continuum between model A and B.

We come to the remarkable result: the model B with the suppressed far UV radiation that was also assumed in the model of Mazzali et al. (1992) recovers the LMC abundance of Ba from the Ba II 6142 Å line. Therefore, we conclude that at present there is no serious reason anymore to suggest the overabundance of Ba in the hydrogen-rich envelope of SN 1987A. The "Ba problem" in SN 1987A was mainly a by-product of the steady-state approximation used for the determination of hydrogen ionization.

5. Discussion and conclusions

Our goal has been to explore the role of time-dependent effects in the ionization and excitation of hydrogen in the atmosphere of SN 1987A. We have developed the model that calculated the time-dependent kinetics of relevant processes together with the time-dependent energy balance. The computations have confirmed our previous conclusion (Utrobin & Chugai 2002) that the effect of the time-dependent ionization in SN 1987A at the photospheric epoch is strong: the hydrogen ionization in the atmosphere is significantly larger and, as a result, the hydrogen excitation is higher as well. The H α formation at the photospheric epoch during the first month is essentially controlled by the time-dependent ionization effect and the additional excitation by the external ^{56}Ni is not needed to account for the strength of H α line.

Although we have failed to reproduce the additional blue peak in the H α line (Bochum event) that emerged between day 20 and 29 (Hanuschik & Dachs 1988), we have found that on day 29.68 one of the models revealed a non-monotonic behavior of the H α optical depth with the positions of maximum and minimum that were suggested by the H α profile at this epoch. This result raises a hope that the blue peak will be explained in a more advanced time-dependent model with a correct treatment of the UV radiation transfer.

At the epoch preceding the Bochum event the time-dependent model produces the realistic distribution of the hydrogen fractional ionization in the atmosphere. With this structure we are able to reproduce the Ba II 6142 Å line in SN 1987A on day 14.68 and 19.68 with the LMC abundance of Ba. We believe, therefore, that the Ba problem, i.e., unacceptably high Ba overabundance in SN 1987A, is resolved. The missing physics of the former models is identified: the time-dependent ionization that provides a higher electron concentration in the atmosphere and thus more efficient recombination of Ba III into Ba II compared to the steady-state models.

Acknowledgements. V.P.U. is grateful to Wolfgang Hillebrandt and Ewald Müller for hospitality during staying at the MPA, and also would like to thank Manuel Bautista and Keith Butler for kindly providing him with the photoionization cross sections of singly ionized iron and barium, respectively. N.N.C. thanks Roger Chevalier for hospitality in Department of Astronomy of the University of Virginia, where a part of this work has been done. This work has been supported in part by the Russian Foundation for Fundamental Research (01-02-16295).

Appendix A: Atomic data

A.1. Hydrogen

For hydrogen we use a model atom consisting of 15 levels all of them being treated as single levels. The energy levels and oscillator strengths for the all transitions are taken from Wiese et al. (1966). The radiative probability of the hydrogen 2s–1s two-photon transition and the distribution of the hydrogen two-photon continuum are given by Nussbaumer & Schmutz (1984). The photoionization cross sections of hydrogen are computed with the formulae and tables of Karzas & Latter (1961). The temperature-averaged free-free Gaunt factor is interpolated from the table and accurate extrapolations given by Sutherland (1998). The electron collisional excitation and deexcitation rates for atomic hydrogen are calculated with the effective collision strengths taken from Scholz et al. (1990), Callaway (1994), Aggarwal et al. (1991), and Giovanardi et al. (1987). The electron collisional ionization rates for atomic hydrogen are calculated using the approximate formulae of Johnson (1972). The rate coefficients for charge transfer in collisions of O $^+$ with H and H $^+$ with O are given by Stancil et al. (1999).

A.2. Singly ionized magnesium

For singly ionized magnesium we use a model ion consisting of 9 single levels. The energy levels and oscillator strengths for the all transitions are compiled from the Atomic Spectroscopic Database (ASD) at the National Institute of Standards and Technology (NIST) and from Kurucz & Bell (1995). The photoionization cross sections of ionized magnesium are taken from the Opacity Project atomic database (Cunto et al. 1993). The effective collision strengths for the electron excitation of ionized magnesium were computed by Sigut & Pradhan (1995). The electron collisional ionization rates for singly ionized magnesium are evaluated by fits of Voronov (1997), the approximate formula of Milkey & Mihalas (1974), and the semi-empirical formula of Lotz (1969).

A.3. Singly ionized iron

For the specific case of the Fe II ion a 30-term, multilevel atom model is employed. A total number of 212 transitions between these terms from 2150 Å to 55 μm are calculated. The energy levels and oscillator strengths for the all transitions in singly ionized iron are compiled from ASD at NIST and from Kurucz & Bell (1995). The photoionization cross sections of ionized iron are taken from Nahar & Pradhan (1994) and Bautista & Pradhan (1998), and averaged over resonance structures according to Bautista et al. (1998). The Maxwellian averaged rate coefficients for the infrared, optical and ultraviolet transitions in ionized iron are taken from Zhang & Pradhan (1995). The collision strengths for some transitions are calculated by using an empirical formula derived from the available experimental and theoretical data for Fe II (Li et al. 1993). The rate of direct collisional ionization for singly ionized iron from the ground state is computed using the fits from Voronov (1997)

and the electron collisional ionization rates from excited levels are evaluated by the semi-empirical formula of Lotz (1969).

A.4. Singly ionized barium

For the case of the Ba II ion a 17-term, multilevel atom model is used with a total number of 56 transitions between these terms from 1500 Å to 58 μm. The energy levels and oscillator strengths for the all transitions in singly ionized barium are taken from Kurucz & Bell (1995). The photoionization cross sections of ionized barium are given by Butler (2000) and averaged over resonance structures according to Bautista et al. (1998). The electron collisional excitation rates for ionized barium are taken from Schönig & Butler (1998) and compiled from Sobelman et al. (1981) and Van Regemorter (1962). The electron collisional ionization rates are evaluated by the semi-empirical formula of Lotz (1969).

A.5. Other atoms and ions

The following elements are included in the non-steady study: He, C, N, O, Ne, Na, Mg, Si, S, Ar, Ca, Fe, and Ba. All elements are treated with the three ionization stages. The atoms and ions are assumed to consist of the ground state and continuum except the singly ionized elements with a detailed energy level structure. Atomic weights and ionization potentials are from Allen (1973). The partition functions are calculated with the polynomial approximation fit obtained by Irwin (1981). The photoionization cross sections of atoms and ions are evaluated with data of Verner & Yakovlev (1995) and Verner et al. (1996). As for H the temperature-averaged free-free Gaunt factor is taken from Sutherland (1998). The free-free absorption coefficient is calculated with the effective nuclear charge including screening effects (Sutherland & Dopita 1993). The electron collisional ionization rates for atoms and ions are computed using the approximate formulae of Voronov (1997).

Appendix B: Molecular data

B.1. Negative hydrogen ion

The photoionization cross section data for negative hydrogen ion are taken from Wishart (1979). The free-free absorption coefficient of negative hydrogen ion was calculated by Bell & Berrington (1987).

B.2. Other hydrogen molecules

The neutral-neutral reactions for hydrogen molecules are listed in Table B.1 with their names and references from which the corresponding rate coefficients are taken. Tables B.2 and B.3 list the ion-neutral and ion-ion reactions for hydrogen molecules with the relevant references, respectively. The electron reactions for hydrogen molecules are listed in Table B.4 with their names and references from which the corresponding rate coefficients are taken. Table B.5 gives the photoionization and photodissociation processes, their names, and references from which the photoionization and photodissociation

Table B.1. List of neutral-neutral reactions.

No.	Reaction	Source
1	$H + H \rightarrow H^+ + H + e^-$	Hollenbach & McKee 1989
2	$H + H \rightarrow H^+ + H^-$	Hollenbach & McKee 1989
3	$H + H + H \rightarrow H_2 + H$	Palla et al. 1983
4	$H + H + H_2 \rightarrow 2H_2$	Palla et al. 1983
5	$H(2s) + H \rightarrow H_2^+ + e^-$	Rawlings et al. 1993
6	$H(2p) + H \rightarrow H_2^+ + e^-$	Rawlings et al. 1993
7	$H(3) + H \rightarrow H_2^+ + e^-$	Rawlings et al. 1993
8	$H(2s) + H(1s) \rightarrow H_2 + \gamma$	Latter & Black 1991
9	$H(2p) + H(1s) \rightarrow H_2 + \gamma$	Latter & Black 1991
10	$H + H_2 \rightarrow 3H$	Roberge & Dalgarno 1982
11	$H + H_2 \rightarrow H^- + H_2^+$	Hollenbach & McKee 1989
12	$H + H_2 \rightarrow H_2^+ + H + e^-$	Hollenbach & McKee 1989
13	$H + H_2 \rightarrow H^+ + H_2 + e^-$	Hollenbach & McKee 1989
14	$H^+ + H_2 \rightarrow H_3^+ + e^-$	Culhane & McCray 1995
15	$H_2 + H_2 \rightarrow H_3^+ + H_2 + e^-$	Hollenbach & McKee 1989
16	$H_2 + H_2 \rightarrow H_2 + 2H$	Rawlings 1988

Table B.2. List of ion-neutral reactions.

No.	Reaction	Source
17	$H^- + H \rightarrow 2H + e^-$	Abel et al. 1997
18	$H^- + H \rightarrow H_2 + e^-$	Galli & Palla 1998
19	$H^+ + H \rightarrow H_2^+ + \gamma$	Galli & Palla 1998
20	$H^+ + H_2 \rightarrow H_3^+ + \gamma$	Galli & Palla 1998
21	$H^+ + H_2 \rightarrow H_2^+ + H$	Galli & Palla 1998
22	$H_2^+ + H \rightarrow H_2 + H^+$	Galli & Palla 1998
23	$H_2^+ + H_2 \rightarrow H_3^+ + H$	Hollenbach & McKee 1989
24	$H_2^+ + H_2 \rightarrow H_2 + H^+ + H$	Hollenbach & McKee 1989
25	$H_3^+ + H \rightarrow H_2 + H_2^+$	Galli & Palla 1998
26	$H_3^+ + H_2 \rightarrow H_2 + H_2^+ + H$	Hollenbach & McKee 1989
27	$H_3^+ + H_2 \rightarrow 2H_2 + H^+$	Hollenbach & McKee 1989

Table B.3. List of ion-ion reactions.

No.	Reaction	Source
28	$H^- + H^+ \rightarrow 2H$	Galli & Palla 1998
29	$H^- + H^+ \rightarrow H_2^+ + e^-$	Galli & Palla 1998
30	$H^- + H_2^+ \rightarrow H + H_2$	Abel et al. 1997

cross sections are taken. These cross sections are used in calculating the ionization and dissociation rates in the radiation field presented in Sect. 3.1.

Appendix C: Rate equations for H^+ , H^- , H_2 , H_2^+ , and H_3^+

Using the physical values and quantities from Sect. 3.5 the rate equation for ionized hydrogen may be written as

$$\frac{\partial N_{H^+}}{\partial t} = -\frac{N_{H^+}}{t_{exp}} + \sum_{k=1}^{15} R_{k,c}^{\gamma} + \sum_{k=1}^{15} N_{H^0,k} P_k - N_{H^+} N_e \sum_{k=2}^{15} \alpha_k$$

Table B.4. List of electron reactions.

No.	Reaction	Source
31	$e^- + H^- \rightarrow H + 2e^-$	Abel et al. 1997
32	$e^- + H_2 \rightarrow 2H + e^-$	Stibbe & Tennyson 1999
33	$e^- + H_2 \rightarrow H + H^-$	Fuller & Couchman 2000
34	$e^- + H_2 \rightarrow H_2^+ + 2e^-$	Hollenbach & McKee 1989
35	$e^- + H_2^+ \rightarrow 2H$	Galli & Palla 1998
36	$e^- + H_3^+ \rightarrow H + H_2$	Galli & Palla 1998
37	$e^- + H_3^+ \rightarrow 3H$	Hollenbach & McKee 1989

Table B.5. List of photoionization and photodissociation processes.

No.	Process	Source
1	$H_2 + \gamma \rightarrow H_2^+ + e^-$	Yan et al. 1998, 2001
2	$H_2 + \gamma \rightarrow 2H$	Abel et al. 1997
3	$H_2 + \gamma \rightarrow H_2^+ + 2H$	Abel et al. 1997
4	$H_2^+ + \gamma \rightarrow H + H^+$	Stancil 1994
5	$H_2^+ + \gamma \rightarrow 2H^+ + e^-$	Shapiro & Kang 1987

$$\begin{aligned}
& + N_e \sum_{k=1}^{15} N_{H^0,k} q_{k,c} - N_{H^+} N_e^2 \sum_{k=1}^{15} q_{c,k} \\
& + (k_1 + k_2) N_{H^0}^2 + k_{13} N_{H^0} N_{H_2} \\
& + k_{22} N_{H_2^+} N_{H^0} + k_{24} N_{H_2^+} N_{H_2} + k_{27} N_{H_3^+} N_{H_2} \\
& + k_{OH} N_{O^+} N_{H^0} + (R_4 + 2R_5) N_{H_2^+} \\
& - k_{19} N_{H^+} N_{H^0} - (k_{20} + k_{21}) N_{H^+} N_{H_2} \\
& - (k_{28} + k_{29}) N_{H^-} N_{H^+} - k_{HO} N_{H^+} N_{O^0}, \quad (C.1)
\end{aligned}$$

where R_4 and R_5 are the photodissociation and dissociative photoionization rates evaluated with the relevant cross sections from Table B.5, respectively; the rate coefficients for the involved reactions are taken from Tables B.1–B.3. Radiative recombinations to the ground state of hydrogen lead to immediate reionizations from the ground state, so they are omitted. The rate equation for negative hydrogen ion is

$$\begin{aligned}
\frac{\partial N_{H^-}}{\partial t} &= -\frac{N_{H^-}}{t_{exp}} + N_{H^0} N_e \alpha_{H^-} - N_{H^-} P_{H^-} \\
& + k_2 N_{H^0}^2 + k_{11} N_{H^0} N_{H_2} + k_{33} N_e N_{H_2} \\
& - (k_{17} + k_{18}) N_{H^-} N_{H^0} - k_{30} N_{H^-} N_{H_2^+} \\
& - (k_{28} + k_{29}) N_{H^-} N_{H^+} - k_{31} N_e N_{H^-}, \quad (C.2)
\end{aligned}$$

where α_{H^-} and P_{H^-} are the total coefficient of photo-attachment of neutral hydrogen and electron to negative hydrogen ion and the photo-detachment rate of negative hydrogen ion in the continuum radiation field, respectively; the rate coefficients for the corresponding reactions are taken from Tables B.1–B.4. The rate equation for molecular hydrogen H_2 is given by

$$\begin{aligned}
\frac{\partial N_{H_2}}{\partial t} &= -\frac{N_{H_2}}{t_{exp}} - (R_1 + R_2 + R_3) N_{H_2} \\
& + k_3 N_{H^0}^3 + k_4 N_{H^0}^2 N_{H_2} \\
& + k_8 N_{H^0,1} N_{H^0,2s} + k_9 N_{H^0,1} N_{H^0,2p} \\
& + k_{18} N_{H^-} N_{H^0} + k_{22} N_{H_2^+} N_{H^0} + k_{25} N_{H_3^+} N_{H^0}
\end{aligned}$$

$$\begin{aligned}
& + k_{27} N_{H_3^+} N_{H_2} + k_{30} N_{H^-} N_{H_2^+} + k_{36} N_e N_{H_3^+} \\
& - (k_{10} + k_{11} + k_{12}) N_{H^0} N_{H_2} \\
& - k_{14} N_{H_2} N_{H^0} - (k_{15} + k_{16}) N_{H_2}^2 \\
& - (k_{20} + k_{21}) N_{H^+} N_{H_2} - k_{23} N_{H_2^+} N_{H_2} \\
& - (k_{32} + k_{33} + k_{34}) N_e N_{H_2}, \quad (C.3)
\end{aligned}$$

where R_1 , R_2 , and R_3 are the photoionization, direct photodissociation, and two-step photodissociation (the Solomon process) rates of molecular hydrogen H_2 evaluated with the cross sections from Table B.5, respectively; the rate coefficients for the involved reactions are taken from Tables B.1–B.4. Finally, the rate equations for molecular hydrogen H_2^+ and H_3^+ are

$$\begin{aligned}
\frac{\partial N_{H_2^+}}{\partial t} &= -\frac{N_{H_2^+}}{t_{exp}} + R_1 N_{H_2} - (R_4 + R_5) N_{H_2^+} \\
& + (k_5 N_{H^0,2s} + k_6 N_{H^0,2p} + k_7 N_{H^0,3}) N_{H^0} \\
& + (k_{11} + k_{12}) N_{H^0} N_{H_2} + k_{15} N_{H_2}^2 \\
& + k_{19} N_{H^+} N_{H^0} + k_{21} N_{H^+} N_{H_2} + k_{25} N_{H_3^+} N_{H^0} \\
& + k_{26} N_{H_3^+} N_{H_2} + k_{29} N_{H^-} N_{H^+} + k_{34} N_e N_{H_2} \\
& - k_{22} N_{H_2^+} N_{H^0} - (k_{23} + k_{24}) N_{H_2^+} N_{H_2} \\
& - k_{30} N_{H^-} N_{H_2^+} - k_{35} N_e N_{H_2^+} \quad (C.4)
\end{aligned}$$

and

$$\begin{aligned}
\frac{\partial N_{H_3^+}}{\partial t} &= -\frac{N_{H_3^+}}{t_{exp}} + k_{14} N_{H_2} N_{H^0} \\
& + k_{20} N_{H^+} N_{H_2} + k_{23} N_{H_2^+} N_{H_2} \\
& - k_{25} N_{H_3^+} N_{H^0} - (k_{26} + k_{27}) N_{H_3^+} N_{H_2} \\
& - (k_{36} + k_{37}) N_e N_{H_3^+}, \quad (C.5)
\end{aligned}$$

respectively.

References

- Abel, T., Anninos, P., Zhang, Y., & Norman, M. L. 1997, *New Astron.*, 2, 181
- Aggarwal, K. M., Berrington, K. A., Burke, P. G., Kingston, A. E., & Pathak, A. 1991, *J. Phys. B: Atom. Molec. Opt. Phys.*, 24, 1385
- Allen, C. W. 1973, *Astrophysical Quantities* (Athlone Press, London)
- Bautista, M. A., & Pradhan, A. K. 1998, *ApJ*, 492, 650
- Bautista, M. A., Romano, P., & Pradhan, A. K. 1998, *ApJS*, 118, 259
- Bell, K. L., & Berrington, K. A. 1987, *J. Phys. B: Atom. Molec. Phys.*, 20, 801
- Butler, K. 2000, private communication
- Callaway, J. 1994, *At. Data Nucl. Data Tables*, 57, 9
- Castor, J. I. 1970, *MNRAS*, 149, 111
- Catchpole, R. M., Menzies, J. M., Monk, A. S., et al. 1987, *MNRAS*, 229, 15P
- Catchpole, R. M., Whitelock, P. A., Feast, M. W., et al. 1988, *MNRAS*, 231, 75P
- Chandrasekhar, S. 1934, *MNRAS*, 94, 444
- Chugai, N. N. 1980, *SvAL*, 6, 91
- Chugai, N. N. 1991a, in *Supernovae*, ed. S. E. Woosley (New York: Springer-Verlag), 286
- Chugai, N. N. 1991b, *SvAL*, 17, 400
- Chugai, N. N., & Utrobin, V. P. 2000, *A&A*, 354, 557
- Clayton, D. D., Leising, M. D., The, L.-S., Johnson, W. N., & Kurfess, J. D. 1992, *ApJ*, 399, L141
- Culhane, M., & McCray, R. 1995, *ApJ*, 455, 335

- Cunto, W., Mendoza, C., Ochsenbein, F., & Zeppen, C. J. 1993, *A&A*, 275, L5
- Dufour, R. J. 1984, in *IAU Symp. 108: Structure and Evolution of the Magellanic Clouds*, ed. S. van den Bergh & K. S. de Boer (Dordrecht: Reidel), 353
- Eastman, R. G., & Kirshner, R. P. 1989, *ApJ*, 347, 771
- Fransson, C., & Kozma, C. 1993, *ApJ*, 408, L25
- Fuller, T. M., & Couchman, H. M. P. 2000, *ApJ*, 544, 6
- Galli, D., & Palla, F. 1998, *A&A*, 335, 403
- Gear, C. W. 1971, *Numerical initial value problems in ordinary differential equations* (Prentice-Hall, New Jersey)
- Giovanardi, C., Natta, A., & Palla, F. 1987, *A&AS*, 70, 269
- Hamuy, M., Suntzeff, N. B., Gonzalez, R., & Martin, G. 1988, *AJ*, 95, 63
- Hauschik, R. W., & Dachs, J. 1988, *A&A*, 205, 135
- Hollenbach, D. J., & McKee, C. F. 1989, *ApJ*, 342, 306
- Irwin, A. W. 1981, *ApJS*, 45, 621
- Jeffery, D. J. 1993, *ApJ*, 415, 734
- Jeffery, D. J. 1995, *ApJ*, 440, 810
- Johnson, L. C. 1972, *ApJ*, 174, 227
- Karzas, W. J., & Latter, R. 1961, *ApJS*, 6, 167
- Kirshner, R. P., & Kwan, J. 1975, *ApJ*, 197, 415
- Kozma, C., & Fransson, C. 1992, *ApJ*, 390, 602
- Kurucz, R. L., & Bell, B. 1995, *Atomic Line Data*, Kurucz CD-ROM No. 23 (Cambridge, Mass.: Smithsonian Astrophysical Observatory)
- Latter, W. B., & Black, J. H. 1991, *ApJ*, 372, 161
- Li, H., McCray, R., & Sunyaev, R. A. 1993, *ApJ*, 419, 824
- Lotz, W. 1969, *Zs. Physik*, 220, 466
- Lundqvist, P., & Fransson, C. 1996, *ApJ*, 464, 924
- Mazzali, P. A., Lucy, L. B., & Butler, K. 1992, *A&A*, 258, 399
- Meaburn, J., Bryce, M., & Holloway, A. J. 1995, *A&A*, 299, L1
- Michael, E., McCray, R., Chevalier, R., et al. 2003, *ApJ*, 593, 809
- Mihalas, D. 1978, *Stellar Atmospheres* (Freeman, San-Francisco)
- Milkey, R. W., & Mihalas, D. 1974, *ApJ*, 192, 769
- Mitchell, R. C., Baron, E., Branch, D., et al. 2002, *ApJ*, 574, 293
- Nahar, S. N., & Pradhan, A. K. 1994, *Phys. Rev. A*, 46, 1916
- Nussbaumer, H., & Schmutz, W. 1984, *A&A*, 138, 495
- Palla, F., Salpeter, E. E., & Stahler, S. W. 1983, *ApJ*, 271, 632
- Phillips, M. M., Heathcote, S. R., Hamuy, M., & Navarrete, M. 1988, *AJ*, 95, 1087
- Prantzos, N., Hashimoto, M., & Nomoto, K. 1990, *A&A*, 234, 211
- Pun, C. S. J., Kirshner, R. P., Sonneborn, G., et al. 1995, *ApJS*, 99, 223
- Rawlings, J. M. C. 1988, *MNRAS*, 232, 507
- Rawlings, J. M. C., Drew, J. E., & Barlow, M. J. 1993, *MNRAS*, 265, 968
- Roberge, W., & Dalgarno, A. 1982, *ApJ*, 225, 176
- Scholz, T. T., Walters, H. R. J., Burke, P. G., & Scott M. P. 1990, *MNRAS*, 242, 692
- Schöning, T., & Butler, K. 1998, *A&AS*, 128, 581
- Shapiro, P. R., & Kang, H. 1987, *ApJ*, 318, 32
- Sigut, T. A. A., & Pradhan, A. K. 1995, *J. Phys. B: Atom. Molec. Phys.*, 28, 4879
- Sobelman, I. I., Vainshtein, L. A., & Yukov, E. A. 1981, *Excitation of Atoms and Broadening of Spectral Lines*. Springer Series Chem. Phys. 7 (Springer, Berlin)
- Sobolev, V. V. 1960, *Moving Envelopes of Stars* (Harvard University Press, Cambridge)
- Stancil, P. C. 1994, *ApJ*, 430, 360
- Stancil, P. C., Schultz, D. R., Kimura, M., et al. 1999, *A&AS*, 140, 225
- Stibbe, D. T., & Tennyson, J. 1999, *ApJ*, 513, L147
- Sutherland, R. S. 1998, *MNRAS*, 300, 321
- Sutherland, R. S., & Dopita, M. A. 1993, *ApJS*, 88, 253
- Utrobin, V. P. 2004, *Astron. Lett.*, 30, 293
- Utrobin, V. P., & Chugai, N. N. 2002, *Astron. Lett.*, 28, 386
- Utrobin, V. P., Chugai, N. N., & Andronova, A. A. 1995, *A&A*, 295, 129
- Van Regemorter, H. 1962, *ApJ*, 136, 906
- Verner, D. A., & Yakovlev, D. G. 1995, *A&AS*, 109, 125
- Verner, D. A., Ferland, G. J., Korista, K. T., & Yakovlev, D. G. 1996, *ApJ*, 465, 487
- Voronov, G. S. 1997, *At. Data Nucl. Data Tables*, 65, 1
- Wang, L. 1991, *A&A*, 246, L69
- Weymann, R. 1966, *ApJ*, 145, 560
- Wiese, W. L., Smith, M. W., & Glennon, B. M. 1966, *Atomic Transition Probabilities. Volume I. Hydrogen Through Neon* (NSRDS-NBS 4)
- Wishart, A. W. 1979, *MNRAS*, 187, 59P
- Woosley, S.E., & Weaver, T.A. 1995, *ApJS*, 101, 181.
- Woosley, S. E., Heger, A., Weaver, T. A., & Langer, N. 1997, in *SN 1987A: Ten Years Later*, ed. M. M. Phillips, & N. B. Suntzeff, in press
- Yan, M., Sadeghpour, H. R., & Dalgarno, A. 1998, *ApJ*, 496, 1044
- Yan, M., Sadeghpour, H. R., & Dalgarno, A. 2001, *ApJ*, 559, 1194
- Zeldovich, Ya. B., Kurt, V. G., & Sunyaev, R. A. 1968, *JETP*, 55, 278
- Zhang, H. L., & Pradhan, A. K. 1995, *A&A*, 293, 953